(Received 3 January 2024, Accepted 23 February 2024, Scheduled 2 March 2024)

Research on Circular Polarization Composite Scattering Characteristics of Sea Surface and Ship Target at GPS Frequency

Ye Zhao*, Long-Wen Liao, Ya-Jie Liu, Wei Tian, Xin-Cheng Ren, and Peng-Ju Yang

School of Physics and Electronic Information, Yan'an University, Yan'an 716000, China

ABSTRACT: The electromagnetic characteristics analysis of the scattering signals from targets, which usually exist or are hidden in the surrounding environment, is one of the necessary prerequisites for the reliable reception of echo signals. Utilizing the GNSS signals as an opportunistic illumination source for detecting maritime targets has vast development prospect and scientific application value. GNSS signals, including GPS signals, are the right-hand circular polarization waves at L-band. Therefore, in this study, a comprehensive electromagnetic composite scattering model is established under circular polarization, which encompasses sea surface scattering, target single scattering, target multiple scattering, and coupled scattering between the target and sea surface. Then, the research investigates the variation characteristics of different scattering components (including the scattering of sea surface, the first, second, and third-order scattering of target, the total scattering of target, the coupled scattering of target induced by the reflection waves from sea surface, and the coupled scattering of sea surface induced by the reflection waves from target) in the composite scene under different polarizations, incident angles, wind speeds, and headings. The results indicate that the scattering of sea surface under LR polarization (which means that the polarization states of scattering and incident wave are left-hand circular polarization (LHCP) and right-hand circular polarization (RHCP), respectively) is significantly greater than that under RR polarization, while the opposite trend is observed for the target. Therefore, in the applications such as the detection and identification of ship targets on sea surface, it is better to choose the right-hand circular polarization channel to receive the scattering echo signal from target, which could effectively suppress the scattering echo of sea surface. These findings are of crucial significance in enhancing the effectiveness and accuracy of maritime target detection.

1. INTRODUCTION

Detecting the state of ocean, such as sensing sea ice, ocean wind retrieval, salinity retrieval, wave height retrieval, or detecting radar targets on ocean requires a comprehensive set of data. In practical terms, the investigation and analysis of the electromagnetic (EM) composite scattering between the radar targets and sea surface hold significant practical importance for both the sea surface and maritime targets. Increasingly, more countries are emphasizing the development of marine resources, the monitoring of marine environment, and the detection of marine targets. Numerous scholars have made outstanding achievements in the field of computational electromagnetics [1–4]. At present, the main ways to research on the composite EM scattering between the radar targets and sea surface are three methodologies: numerical methods, approximate methods, and hybrid algorithms.

The principle of the numerical methods is to analyze the target and rough surface as an integrated system. Burkholder et al. introduced a generalized forward-backward (GFB) method to calculate the radar cross section (RCS) of two-dimensional (2-D) ship-like targets on a rough sea surface [5]. The team led by Zhang presented an effective method of fundamental solution (MFS) for numerically simulating composite EM scattering of 2-D object on rough surface [6]. This approach, which is devoid of mesh schemes and singularity analysis, allows for the direct derivation of the desired field based on the fundamental solution of the relevant wave equation. Cloak et al. [7] presented the multiple sweep method of moments (MSMM), which is the first attempt to numerically solve three dimensional (3-D) targets on the ocean-like rough surfaces. Zhang et al. [8] introduced the mode-expansion method, which requires 6% fewer unknowns than the traditional moment of method (MoM), to calculate 2-D EM wave scattering from perfectly electric conducting (PEC) objects on rough ocean surfaces. The accuracy of this method was validated by the iterative MoM, and it successfully addressed various challenges in the solutions. Kuang and Jin [9] proposed a numerical finite-difference time-domain method for EM scattering calculation from a target on rough surface. Wei et al. [10] presented the extension of an efficient multiregion model using the single integral equation (SIE) method. This method enables the calculation of EM scattering from dielectric rough surfaces, regardless of the presence of PEC targets on the rough surface.

The underlying principle of the approximate methods is to decompose the overall field of composite scattering into three components, namely the target field, sea surface field, and coupled field. Through judicious approximations made under appropriate conditions, these three components can be vector superimposed, yielding the accurate final results. Chiu and Sarabandi [11], as well as Lawrence and Sarabandi [12] proposed

* Corresponding author: Ye Zhao (zhaoye07074135@163.com).

an EM scattering solution for the interaction between a dielectric cylinder and a slightly rough surface using the reciprocity theorem. The four-path model proposed by Johnson [13, 14] is currently the most widely utilized method, which considers the rough surface as a large plane, and the coupling effect between the target and rough surface is replaced by mirror reflections. The four-path model can reasonably predict the coherent scattering. However, it could not calculate the incoherent object/surface interaction effects that can make significant contributions to received cross sections. Burkholder et al. [15, 16] investigated radar scattering issues of targets on a rough sea surface respectively using the methods of iterative physical optics (IPO) and shooting and bouncing rays (SBR). Approximate methods constitute mature and effective computational methods. In general, these methods include geometrical optics (GO) [17], physical optics (PO) [18], iterative physical optics (IPO) [19], geometrical optics and physical optics (GO-PO) [20, 21], bidirectional analytic ray tracing (BART) [22], and others. For these ray methods, the shadowing effects for multiple scattering in the optics field [23–25] should be considered to improve the calculation accuracy.

In the hybrid algorithms, different methods are used to calculate the EM scattering of target and rough surface, then considering the coupling effect between the target and rough surface. In comparison with the alternative methods, the hybrid approaches are demonstrated to have superior calculation efficiency. He and Zhu [26] utilized an efficient hybrid MM-PO method combined with UV technology to calculate the EM scattering of a 2-D PEC target above a rough PEC rough surface, which could effectively solve the scattering challenges associated with large-scale targets on rough surfaces. Guan et al. [27] introduced the Kirchhoff approximation and moment of method (KA-MoM) to analyze the EM scattering from targets above a 2-D PEC rough surface. This hybrid algorithm only needs to discretize the grid of target, so the computational time and memory diminish substantially. Yang et al. [28] explored an iterative hybrid method that integrates the KA with the multilevel fast multipole algorithm (MLFMA), which could provide a robust analysis of the scattering of 3-D objects above a random dielectric rough surface. Bellez et al. [29] proposed an efficient hybrid KA-EFIE formulation for analyzing the EM scattering of a 3-D PEC object buried beneath a 2-D dielectric rough surface. The above researches mainly focus on the linear polarization EM composite scattering characteristics between the target and rough surface with the plane EM wave incidence.

Therefore, the primary objective of this study is to establish a comprehensive EM scattering model that focuses on circular polarization composite scattering characteristics between the sea surface and ship target in a complex scene at GPS frequency of 1.57 GHz. The discussions are centered on the EM scattering characteristics of different scattering components under the conditions of different polarizations, incident angles, wind speeds, and headings, which include the scattering of sea surface, the first, second, and third-order scattering of target, the total scattering of target, the coupled scattering of target induced by the reflection waves from sea surface, and the coupled scattering of sea surface induced by the reflection waves from target. The rest of this paper is organized as follows. Section 2 provides an overview of the modeling of the circular polarization composite EM scattering for the interaction between the target and sea surface, which involves the EM scattering model of sea surface under linear polarization configuration and circular polarization configuration, the EM scattering model of target (This subsection includes single scattering, secondary scattering and multiple scattering), and the coupled EM scattering model for the target and sea surface. Section 3 gives the verification of the proposed computational methods, simulation results, and discussions regarding the EM scattering characteristics of the sea surface and ship target. Finally, the conclusion is presented in Section 4.

2. COMPOSITE EM SCATTERING MODEL FOR THE INTERACTION BETWEEN THE SEA SURFACE AND TARGET

The scattering components between the sea surface and overlying target primarily include sea surface scattering, target single scattering, target multiple scattering (caused by the dihedral or trihedral structure of the target itself), and coupled scattering between the target and sea surface, which could be decomposed into the target-coupled scattering induced by the reflection waves from sea surface impacting the target and sea surface-coupled scattering caused by the reflection waves from target impacting the sea surface, as illustrated in Fig. 1. The EM scattering models for each scattering component are separately introduced below.

2.1. EM Scattering Model of Sea Surface

2.1.1. Linear Polarization Configuration

According to the two-scale composite surface and Bragg resonance assumption, the sea surface can be regarded as a series of small slightly rough facets with capillary waves as their microscopic random roughness [30]. The positions of these small facets are determined by the large-scale sea surface profile $\eta(\mathbf{r})$, as shown in Fig. 2. For a small facet, considering a unit plane wave that propagates along the $x'o'z'$ plane of the local coordinate system, the corresponding scattering amplitude can be expressed as [31].

$$\mathbf{S}_{pq}\left(\mathbf{k}_s, \mathbf{k}_i\right) = \frac{k^2(1-\varepsilon)}{8\pi^2} f_{pq} \iint \zeta(\mathbf{r}') \exp(-i\mathbf{q}_0 \cdot \mathbf{r}')\, \mathrm{d}\mathbf{r}' \quad (1)$$

where $\zeta(\mathbf{r}')$ is the height variation of the micro-rough surface; $\mathbf{q}_0 = k\left(\mathbf{k}_s - \mathbf{k}_i\right)$ is the scattering vector; $\mathbf{k}_i$ and $\mathbf{k}_s$ are the wave propagation vectors of the incident and scattering waves, respectively; k is the wavenumber; ε is the dielectric constant of seawater; f_{pq} is the polarization factor. Subscripts p, q respectively represent the polarization states of the scattering and incident waves, which can be horizontal polarization (h) and vertical polarization (v). The polarization factors can be expressed as [31]

$$f_{hh} = [1 + R_h(\theta_s')][1 + R_h(\theta_i')] \cos\phi_s' \quad (2)$$

$$f_{vh} = [1 - R_v(\theta_s')][1 + R_h(\theta_i')] \cos\theta_s' \sin\phi_s' \quad (3)$$

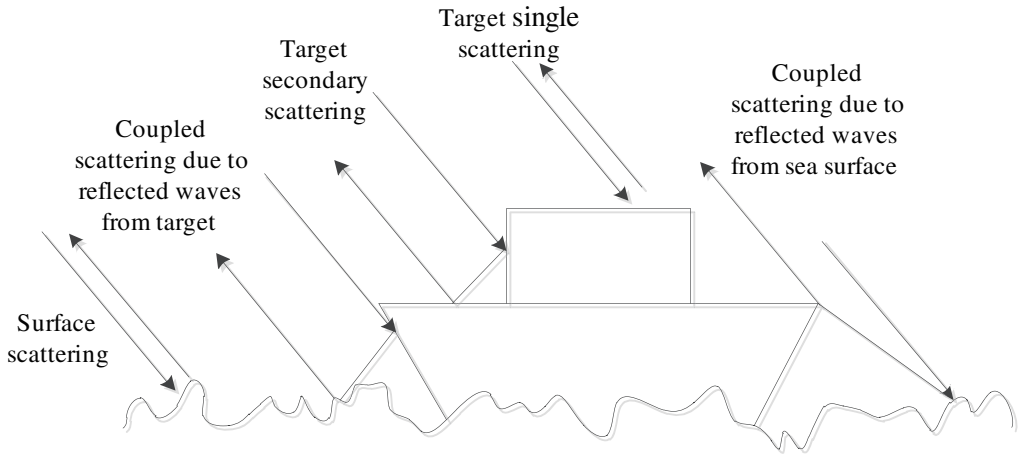

FIGURE 1. Schematic diagram of the scattering components between the sea surface and overlying target.

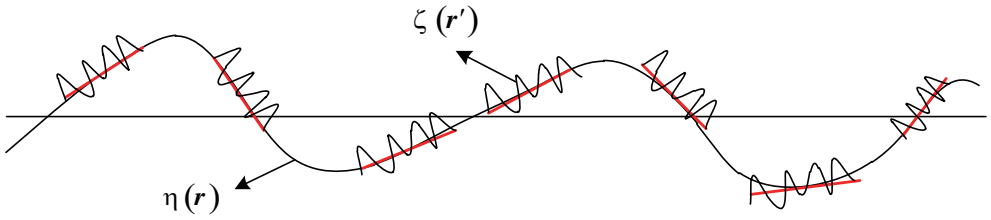

FIGURE 2. Two-scale composite model of the sea surface.

$$f_{vv} = \frac{1}{\varepsilon}[1+R_v(\theta_s')][1+R_v(\theta_i')]\sin\theta_i'\sin\theta_s' - [1-R_v(\theta_s')][1-R_v(\theta_i')]\cos\theta_i'\cos\theta_s'\cos\phi_s' \quad (4)$$

$$f_{hv} = [1+R_h(\theta_s')][1-R_v(\theta_i')]\cos\theta_i'\sin\phi_s' \quad (5)$$

where R_v and R_h are the Fresnel reflection coefficients for vertical and horizontal polarizations, respectively, and θ_i', θ_s', ϕ_s' represent the local angles corresponding to the incident and scattering waves in the local coordinate system. Considering the position of the micro-rough facet in the global coordinate system, the position vector of any point on the rough surface relative to the local coordinate system origin O' is $\mathbf{r}'$, while the position vector of the point relative to the global coordinate system origin O is $\mathbf{r}$. The position vector of the center point O' of the micro-rough facet relative to the global coordinate system origin O is $\mathbf{r}_0$. So we can get $\mathbf{r}' = \mathbf{r} - \mathbf{r}_0$ and $d\mathbf{r}' = d\mathbf{r}$. Thus, in the global coordinate system, the scattering amplitude of an arbitrarily inclined micro-rough facet can be expressed as:

$$\tilde{\mathbf{S}}_{pq}(\mathbf{k}_s, \mathbf{k}_i) = \frac{k^2(1-\varepsilon)}{8\pi^2} e^{-i\mathbf{q}\cdot\mathbf{r}_0} F_{pq} \iint \zeta(\mathbf{r}') \exp(-i\mathbf{q}_0\cdot\mathbf{r}')\, \mathrm{d}\mathbf{r}' \quad (6)$$

The polarization factor F_{pq} in the global coordinate system can be expressed as:

$$\begin{bmatrix} F_{vv} & F_{vh} \\ F_{hv} & F_{hh} \end{bmatrix} = \begin{bmatrix} \widehat{\mathbf{v}}_s\cdot\widehat{\mathbf{v}}_s' & \widehat{\mathbf{v}}_s\cdot\widehat{\mathbf{h}}_s' \\ \widehat{\mathbf{h}}_s\cdot\widehat{\mathbf{v}}_s' & \widehat{\mathbf{h}}_s\cdot\widehat{\mathbf{h}}_s' \end{bmatrix} \begin{bmatrix} f_{vv} & f_{vh} \\ f_{hv} & f_{hh} \end{bmatrix} \begin{bmatrix} \widehat{\mathbf{v}}_i'\cdot\widehat{\mathbf{v}}_i & \widehat{\mathbf{v}}_i'\cdot\widehat{\mathbf{h}}_i \\ \widehat{\mathbf{h}}_i'\cdot\widehat{\mathbf{v}}_i & \widehat{\mathbf{h}}_i'\cdot\widehat{\mathbf{h}}_i \end{bmatrix} \quad (7)$$

where $\widehat{\mathbf{h}}$ and $\widehat{\mathbf{v}}$ represent unit horizontal polarization and vertical polarization vectors. The subscripts "i" and "s" denote the parameters of the incident wave and scattering wave, respectively. The variables with a prime denote unit polarization vectors in the local coordinate system.

Thus, the scattering field of an individual small facet on the sea surface is given by

$$\mathbf{E}_{pq}^{facet}(\mathbf{k}_s, \mathbf{k}_i) = 2\pi\frac{e^{ikR}}{iR}\tilde{\mathbf{S}}_{pq}(\mathbf{k}_i, \mathbf{k}_s) \quad (8)$$

where R represents the distance between the small facet center and observation point. It is important to note that, according to the two-scale composite surface theory, the microroughness profile $\zeta(\mathbf{r}')$ is generated based on the small-scale capillary wave spectrum S^{capi} [32]

$$S^{\text{capi}}(\mathbf{k}) = \begin{cases} S(\mathbf{k}), & |\mathbf{k}| \geq k_{cut} \\ 0, & |\mathbf{k}| \leq k_{cut} \end{cases} \quad (9)$$

where k_{cut} is the cut-off wavenumber, and $S(\mathbf{k})$ is the two-dimensional wave spectrum, which is combined by Elfouhaily's omnidirectional spectrum with the Languet-Higgins directional distribution function.

However, in the specular scattering region, Equation (8) has a strong dependence on the choice of the cut-off wavenumber k_{cut}. The Kirchhoff approximation is an effective method to

calculate the scattering field in the specular scattering region. Therefore, if the sea surface is divided into specular scattering region and diffuse scattering region, Equation (8) can be employed to calculate the scattering field of the facets located in the diffuse scattering region, while the Kirchhoff approximation [33] can be utilized to calculate the scattering field of the facets located in the specular scattering region.

$$\begin{aligned}\mathbf{E}_{pq}^{KA}\left(\mathbf{k}_s,\mathbf{k}_i\right) &= ik\psi_0\widehat{\mathbf{p}}\cdot\widehat{\mathbf{k}}_s\times\iint\left[\left(\widehat{\mathbf{n}}\times\mathbf{E}\right)-\eta\widehat{\mathbf{k}}_s\times\left(\widehat{\mathbf{n}}\times\mathbf{H}\right)\right]\\ &\quad\exp\left(-i\mathbf{q}_0\cdot\mathbf{r}'\right)\mathrm{d}\mathbf{r}'\\ &= ik\psi_0E_0\cdot S_{pq}\cdot\iint\exp\left(-i\mathbf{q}_0\cdot\mathbf{r}'\right)\mathrm{d}\mathbf{r}' \quad (10)\end{aligned}$$

where $\psi_0 = \exp\left(ikR\right)/4\pi R$, η represents the impedance of seawater, while $\mathbf{E}$ and $\mathbf{H}$ denote the total electromagnetic fields on the boundary.

The polarization factor can be expressed as

$$\begin{aligned}S_{pq} &= \widehat{\mathbf{p}}\cdot\left[-\widehat{\mathbf{h}}'_i\left(\widehat{\mathbf{n}}\cdot\widehat{\mathbf{k}}_i\right)\left(\widehat{\mathbf{q}}\cdot\widehat{\mathbf{h}}'_i\right)\left(1-R_h\right)\right.\\ &\quad+\left(\widehat{\mathbf{n}}\times\widehat{\mathbf{h}}'_i\right)\left(\widehat{\mathbf{q}}\cdot\widehat{\mathbf{v}}'_i\right)\left(1+R_v\right)\\ &\quad+\left(\widehat{\mathbf{k}}_s\times\left(\widehat{\mathbf{n}}\times\widehat{\mathbf{h}}'_i\right)\right)\left(\widehat{\mathbf{q}}\cdot\widehat{\mathbf{h}}'_i\right)\left(1+R_h\right)\\ &\quad\left.+\left(\widehat{\mathbf{k}}_s\times\widehat{\mathbf{h}}'_i\right)\left(\widehat{\mathbf{q}}\cdot\widehat{\mathbf{v}}'_i\right)\left(\widehat{\mathbf{n}}\cdot\widehat{\mathbf{k}}_i\right)\left(1-R_v\right)\right] \quad (11)\end{aligned}$$

where $\widehat{\mathbf{n}}$ is the unit normal vector; $\widehat{\mathbf{p}}$ is the unit polarization vector of the scattering wave, taking values of either $\widehat{\mathbf{h}}_s$ or $\widehat{\mathbf{v}}_s$; and $\widehat{\mathbf{q}}$ is the unit polarization vector of the incident wave, taking values of either $\widehat{\mathbf{h}}_i$ or $\widehat{\mathbf{v}}_i$. Therefore, the scattering field of an individual small facet on sea surface can be expressed as

$$\mathbf{E}_{pq}\left(\mathbf{k}_i,\mathbf{k}_s\right)=\begin{cases}\mathbf{E}_{pq}^{KA}\left(\mathbf{k}_s,\mathbf{k}_i\right), & \text{specular region}\\ \mathbf{E}_{pq}^{facet}\left(\mathbf{k}_s,\mathbf{k}_i\right), & \text{non}-\text{specular region}\end{cases} \quad (12)$$

The total field from a whole sea surface could be obtained by the summation of the fields from all the tilted rough facets,

$$\mathbf{E}_{pq}^{sea}\left(\mathbf{k}_s,\mathbf{k}_i,t\right)=\sum_{m=1}^{M}\sum_{n=1}^{N}\mathbf{E}_{pq}\left(\mathbf{k}_s,\mathbf{k}_i\right) \quad (13)$$

where M and N are the numbers of the facets along x and y directions, respectively. If the illuminated area of the sea surface is A, the normalized radar cross section (NRCS) of a single frozen surface sample is readily obtained by

$$\sigma_{pq}\left(\mathbf{k}_s,\mathbf{k}_i,t\right)=\lim_{R\to\infty}\frac{4\pi R^2}{A}\left[\mathbf{E}_{pq}^{sea}\left(\mathbf{k}_s,\mathbf{k}_i,t\right)\mathbf{E}_{pq}^{sea}\left(\mathbf{k}_s,\mathbf{k}_i,t\right)^*\right] \quad (14)$$

2.1.2. Circular Polarization Configuration

The circular polarization scattering field E_c can be expressed in terms of the linear polarization scattering field E_l as [34]

$$E_c=\begin{bmatrix}E_{RR} & E_{RL}\\ E_{LR} & E_{LL}\end{bmatrix}=\frac{1}{2}\begin{bmatrix}1 & i\\ 1 & -i\end{bmatrix}E_l\begin{bmatrix}1 & 1\\ -i & i\end{bmatrix} \quad (15)$$

The GPS satellites transmit right-hand circular polarization (RHCP) waves. Through simple matrix calculation, the left-hand and right-hand circular polarization scattering waves under the RHCP incident wave can be respectively expressed as:

$$E_{LR} = \left(E_{vv}-E_{hh}-iE_{vh}-iE_{hv}\right)/2 \quad (16)$$

$$E_{RR} = \left(E_{vv}+E_{hh}-iE_{vh}+iE_{hv}\right)/2 \quad (17)$$

In the above expressions, E_{vv}, E_{hh}, E_{vh}, E_{hv} represent the scattering field of linear polarization wave. The first subscript of scattering field E denotes the polarization state of the scattering wave, and the second subscript represents the polarization state of the incident wave. For example, the subscript LR indicates that the polarization states of the scattering field and incident field are left-hand circular polarization (LHCP) and right-hand circular polarization (RHCP), respectively.

2.2. EM Scattering Model of Target

2.2.1. Single Scattering

Assuming that a certain patch m on target can be illuminated by the plane electromagnetic wave, the induced electric and magnetic currents on this patch are given by:

$$\begin{aligned}\mathbf{M}_{1,m} &= \widehat{\mathbf{n}}\times\mathbf{E}=\left(\widehat{\mathbf{n}}\times\widehat{\mathbf{h}}'_i\right)\left(\widehat{\mathbf{q}}\cdot\widehat{\mathbf{h}}'_i\right)\left(1+R_h\right)E_0\\ &\quad+\widehat{\mathbf{h}}'_i\left(\widehat{\mathbf{q}}\cdot\widehat{\mathbf{v}}'_i\right)\left(\widehat{\mathbf{n}}\cdot\widehat{\mathbf{k}}_i\right)\left(1-R_v\right)E_0 \quad (18)\end{aligned}$$

$$\begin{aligned}\mathbf{J}_{1,m} &= \widehat{\mathbf{n}}\times\mathbf{H}=\left[\left(\widehat{\mathbf{n}}\times\widehat{\mathbf{h}}'_i\right)\left(\widehat{\mathbf{q}}\cdot\widehat{\mathbf{v}}'_i\right)\left(1+R_v\right)E_0\right.\\ &\quad\left.-\widehat{\mathbf{h}}'_i\left(\widehat{\mathbf{q}}\cdot\widehat{\mathbf{h}}'_i\right)\left(\widehat{\mathbf{n}}\cdot\widehat{\mathbf{k}}_i\right)\left(1-R_h\right)E_0\right]/\eta \quad (19)\end{aligned}$$

In the above formulas

$$\widehat{\mathbf{h}}'_i=\frac{\widehat{\mathbf{k}}_i\times\widehat{\mathbf{n}}}{\left|\widehat{\mathbf{k}}_i\times\widehat{\mathbf{n}}\right|},\ \widehat{\mathbf{v}}'_i=\widehat{\mathbf{h}}'_i\times\widehat{\mathbf{k}}_i \quad (20)$$

According to the Stratton-Chu integral equation [35], the far-field scattering field of the patch m can be expressed as:

$$\begin{aligned}\mathbf{E}_{pq,m}^{1}\left(\mathbf{k}_s,\mathbf{k}_i\right) &= ik\psi_0\widehat{\mathbf{p}}\cdot\widehat{\mathbf{k}}_s\times\iint\left(\mathbf{M}_{1,m}-\eta\widehat{\mathbf{k}}_s\times\mathbf{J}_{1,m}\right)\\ &\quad\exp\left(-i\mathbf{q}_0\cdot\mathbf{r}'\right)\mathrm{d}\mathbf{r}' \quad (21)\end{aligned}$$

The phase integral term in the above expression is calculated using the Gordon method [36]. Thus, the overall single scattering field can be represented as:

$$\mathbf{E}_{pq}^{1}\left(\mathbf{k}_s,\mathbf{k}_i\right)=\sum_{m=1}^{N}\mathbf{E}_{pq,m}^{1}\left(\mathbf{k}_i,\mathbf{k}_s\right)\cdot I_{vis,m} \tag{22}$$

where N represents the total number of patches on the target, and $I_{vis,m}=1$ indicates that the patch m can be illuminated by the incident wave.

2.2.2. Secondary Scattering and Multiple Scattering

If the patch n can be illuminated by the reflected wave from the patch m, the first reflected field $\mathbf{E}_m^{r1}$ of patch m is regarded as the incident field of patch n for the secondary scattering of patch n. And the reflected field $\mathbf{E}_m^{r1}$ can be specifically represented as:

$$\mathbf{E}_m^{r1}=\left[\widehat{\mathbf{h}}'_i(\widehat{\mathbf{q}}\cdot\widehat{\mathbf{h}}'_i)R_h+\left(\widehat{\mathbf{h}}'_i\times\widehat{\mathbf{k}}_{r,m}\right)(\widehat{\mathbf{q}}\cdot\widehat{\mathbf{v}}'_i)R_v\right]E_0 \tag{23}$$

It is evident that the wave vector and polarization vector of the reflected wave from the patch m are given by:

$$\mathbf{k}_{r,m}=\widehat{\mathbf{k}}_i-2\widehat{\mathbf{n}}_m\left(\widehat{\mathbf{k}}_{r,m}\cdot\widehat{\mathbf{n}}_m\right) \tag{24}$$

$$\mathbf{q}_m^r=\widehat{\mathbf{h}}'_i(\widehat{\mathbf{q}}\cdot\widehat{\mathbf{h}}'_i)R_h+\widehat{\mathbf{v}}'_i(\widehat{\mathbf{q}}\cdot\widehat{\mathbf{v}}'_i)R_v \tag{25}$$

Substitute $\widehat{\mathbf{q}}$ with $\mathbf{q}_m^r$, $\widehat{\mathbf{k}}_i$ with $\mathbf{k}_{r,m}$, $\widehat{\mathbf{n}}$ with $\widehat{\mathbf{n}}_n$, then recalculate the equations (18)-(20) to obtain the electric current $\mathbf{J}_{2,nm}$ and magnetic current $\mathbf{M}_{2,nm}$ on patch n induced by the reflected wave of patch m. Therefore, the total induced electromagnetic currents on patch n are represented by $\mathbf{M}_{2,n},\mathbf{J}_{2,n}$.

$$\mathbf{M}_{2,n}=\sum_{m=1}^{N}I_{vis,m}\cdot\mathbf{M}_{2,nm}\cdot I_{vis,nm} \tag{26}$$

$$\mathbf{J}_{2,n}=\sum_{m=1}^{N}I_{vis,m}\cdot\mathbf{J}_{2,nm}\cdot I_{vis,nm} \tag{27}$$

In the above equations, $I_{vis,nm}=1$ represents that the patch n can be illuminated by the reflected wave from the patch m.

In this way, the overall secondary scattering field can be expressed as:

$$\mathbf{E}_{pq}^{2}\left(\mathbf{k}_s,\mathbf{k}_i\right)=\sum_{n=1}^{N}ik\psi_0\widehat{\mathbf{p}}\cdot\widehat{\mathbf{k}}_s\times\iint\left(\mathbf{M}_{2,n}-\eta\widehat{\mathbf{k}}_s\times\mathbf{J}_{2,n}\right)\exp\left(-i\mathbf{q}_0\cdot\mathbf{r}'\right)\mathrm{d}\mathbf{r}' \tag{28}$$

For the third-order scattering, the computational process is analogous to the step of the secondary scattering, while for the case of circular polarization waves, the scattering field of target can also be calculated according to Equation (15).

2.3. Coupled EM Scattering Model for the Sea Surface and Target

The GO-PO method can calculate not only the multiple scattering from target but also the coupled scattering between the target and sea surface. Its computational principles are analogous to those employed in the calculation of the secondary scattering from target. Hence, the coupled scattering contribution between the target and sea surface can be expressed as:

$$\begin{aligned}&\mathbf{E}^{\text{target}\to\text{sea}}\left(\mathbf{k}_s,\mathbf{k}_i\right)\\&=ik\psi_0\sum_{m=1}^{N^s}\widehat{\mathbf{p}}\cdot\widehat{\mathbf{k}}_s\times\iint\left(\sum_{n=1}^{N^t}I_{vis,n}^{t}\cdot\mathbf{M}_{c,mn}^{s}\cdot I_{vis,mn}^{st}\right.\\&\left.-\eta\widehat{\mathbf{k}}_s\times\sum_{n=1}^{N^t}I_{vis,n}^{t}\cdot\mathbf{J}_{c,mn}^{s}\cdot I_{vis,mn}^{st}\right)\cdot\exp\left(-i\mathbf{q}_0\cdot\mathbf{r}'\right)\mathrm{d}\mathbf{r}'\end{aligned} \tag{29}$$

$$\begin{aligned}&\mathbf{E}^{sea\to target}\left(\mathbf{k}_s,\mathbf{k}_i\right)=ik\psi_0\sum_{l=1}^{N^t}\widehat{\mathbf{p}}\cdot\widehat{\mathbf{k}}_s\\&\times\iint\left(-\eta\widehat{\mathbf{k}}_s\times\sum_{m=1}^{N^s}I_{vis,m}^{s}\cdot\mathbf{J}_{c,lm}^{t}\cdot I_{vis,lm}^{ts}\right)\\&\cdot\exp\left(-i\mathbf{q}_0\cdot\mathbf{r}'\right)\mathrm{d}\mathbf{r}'\end{aligned} \tag{30}$$

where $I_{vis,n}^{t}$, $I_{vis,m}^{s}=1$ indicates that the patch n on target and the facet m on sea surface can be illuminated by the incident wave; $I_{vis,mn}^{st}=1$ indicates that the facet m on sea surface can be illuminated by the reflected wave from the patch n on target. $I_{vis,lm}^{ts}=1$ indicates that the patch l on target can be illuminated by the reflected wave from the facet m on sea surface. N^t represents the number of patches on target, and N^s represents the number of facets on sea surface.

3. NUMERICAL RESULTS

The GPS satellites transmit right-hand circular polarization waves and operate at the L-band with two carrier frequencies, namely, $L1=1575.42\,\text{MHz}$ and $L2=1227.6\,\text{MHz}$. Therefore, the simulation frequency in this study is 1.57 GHz, and only the cases of left-hand and right-hand circular polarization scattering fields are discussed when the incident wave is right-hand circular polarization. The geometric structure and dimensional parameters of the ship, as well as the composite scattering between the ship and sea surface, are illustrated in Fig. 3.

3.1. Scattering Characteristics Analysis of Sea Surface

To validate the effectiveness of the scattering model of sea surface proposed in this study, Fig. 4 provides the comparisons of the bistatic scattering coefficient of sea surface simulated by the proposed model, the two-scale model (TSM), and the second-order small slope approximation (SSA-II) [34] under linear and circular polarizations. The incident angle is $\theta_i=45°$; the incident azimuth angle is $\phi_i=0°$; the scattering azimuth angle

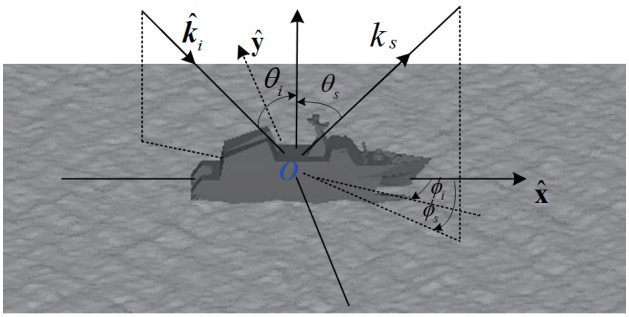

Parameters of ship

Length	46.75 m
Width	12.23 m
Height	12.88 m
Draft	1.5 m

FIGURE 3. The geometric structure of the ship and schematic diagram of the composite scattering.

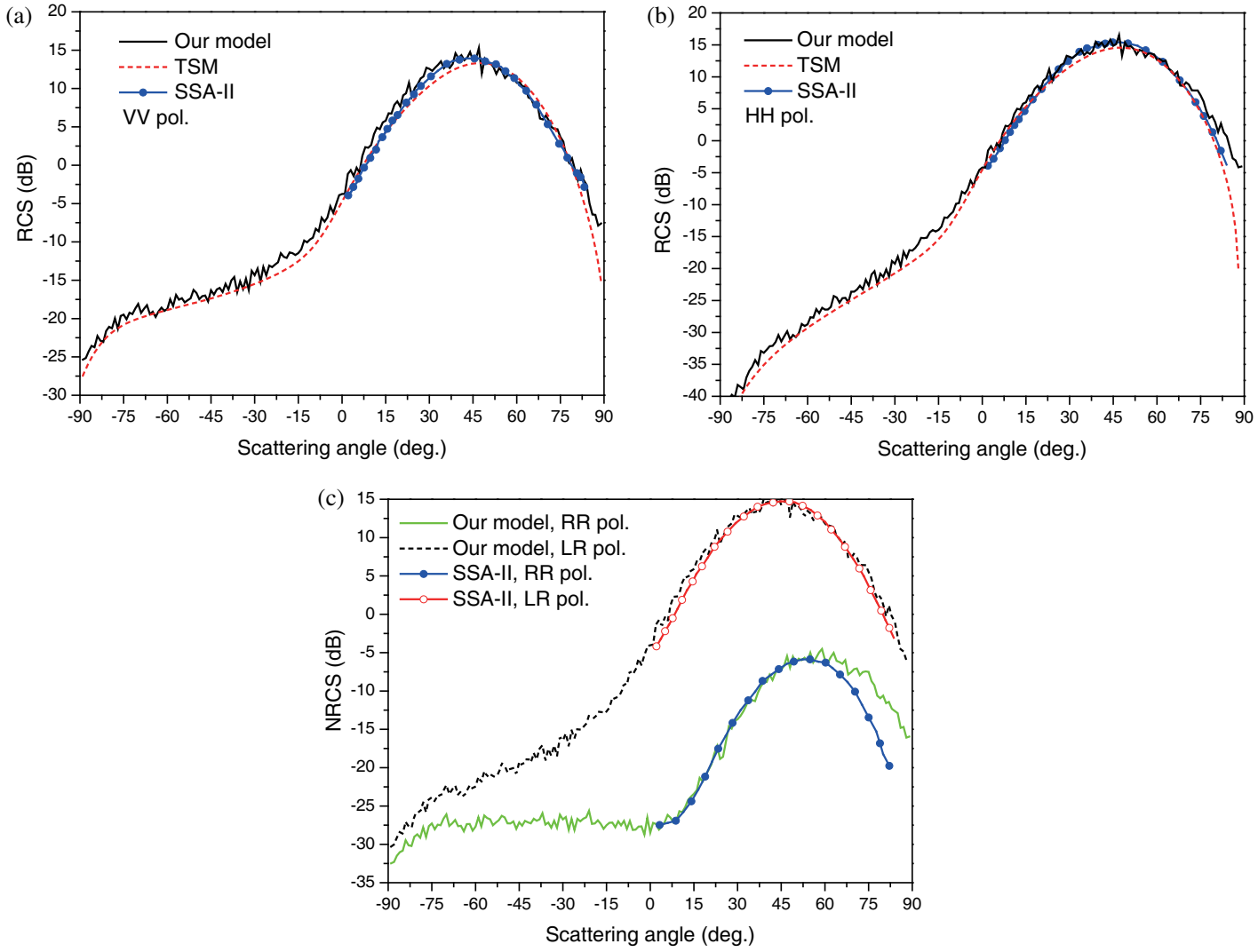

FIGURE 4. Bistatic scattering coefficient verification of sea surface for linear and circular polarization. (a) RCS verification of different methods for VV polarization. (b) RCS verification of different methods for HH polarization. (c) RCS verification of different methods for RR and LR polarization.

is $\phi_s = 0°$; the sea surface grid size is 1.0 m ×1.0 m; the number of sampling points is 128 ×128; the wind speed is 10 m/s; the wind direction is 0°; the seawater temperature is $T = 20\,°\mathrm{C}$; and the salinity is $S = 35$ ppt. It can be observed that the results of the three methods agree exceptionally well for the VV and HH polarizations in Figs. 4(a) and (b). In Fig. 4(c), the result of our model agrees well with the SSA-II for the LR polarization, but for the RR polarization, the difference is relatively large in the forward direction.

Figure 5 presents a comparison of scattering coefficient of sea surface between linear polarization and circular polarization. It can be observed that near the specular direction, the

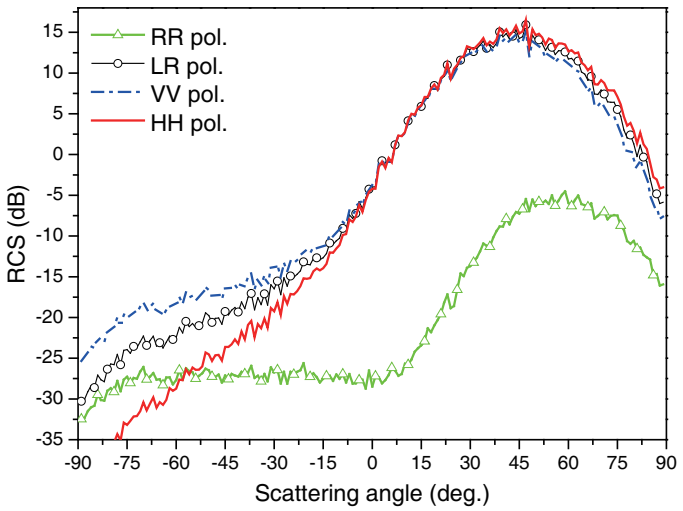

FIGURE 5. RCS comparison of sea surface between linear and circular polarizations.

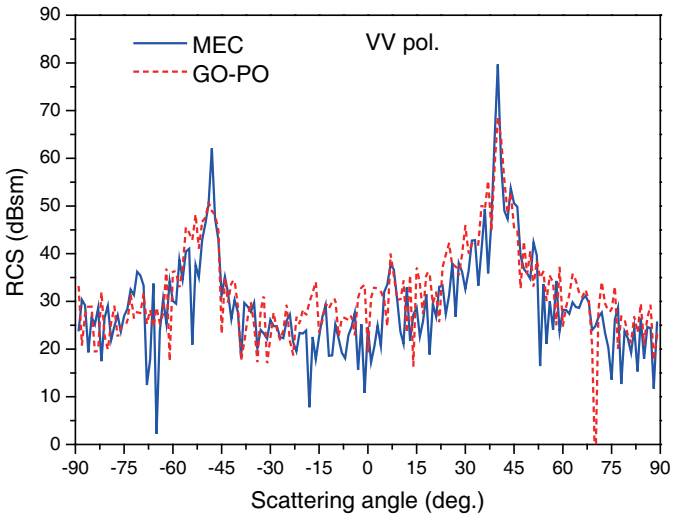

FIGURE 6. RCS verification of ship target for linear polarization.

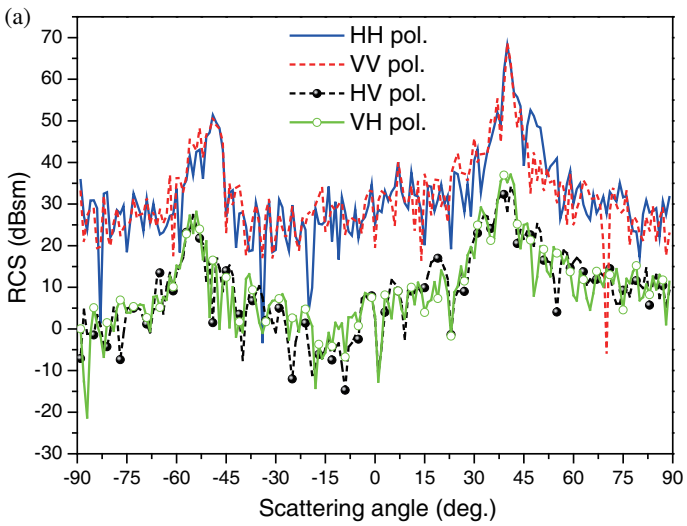

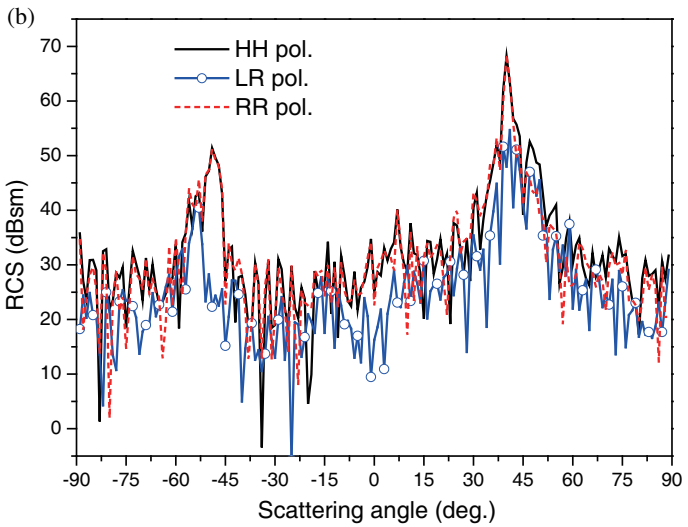

FIGURE 7. Bistatic RCS of ship target under linear and circular polarizations. (a) Linear polarization. (b) Circular polarization.

scattering coefficient for HH polarization is greater than that for VV polarization. However, beyond the specular direction, the scattering coefficient for VV polarization surpasses that for HH polarization. For circular polarization incident waves, the scattering coefficient curve for LR polarization falls between the curves of HH and VV polarizations. In addition, the scattering coefficient of LR polarization significantly exceeds that of RR polarization, which is because of the Brewster effect [37]. When the incident angle is much smaller than the Brewster angle of the rough sea surface, the scattering wave is mainly left-hand circular polarization wave component.

3.2. Scattering Characteristics Analysis of Ship Target

To validate the effectiveness of the GO-PO method in calculating the scattering field of target, Fig. 6 gives a comparison for the RCS of ship target calculated using the method of equivalent currents (MEC) and the GO-PO method under VV polarization. The incident angle is $\theta_i = 40°$; the incident azimuth angle is $\phi_i = 0°$; and the scattering azimuth angle is $\phi_s = 0°$. From Fig. 6, it can be observed that the result obtained by the GO-PO method closely matches that of MEC on the whole. However, at some scattering angles, the results of the GO-PO method are slightly higher than that of MEC, which is because the multiple scatterings are considered in the GO-PO method.

Figure 7 illustrates the bistatic RCS of ship target under linear and circular polarizations. From Fig. 7(a), it can be observed that the RCS of ship for HH polarization is basically consistent with that for VV polarization, and the conclusion is also applicable to the cross-polarizations. However, the RCS under the co-polarizations is significantly greater than the RCS under the cross-polarizations. From Fig. 7(b), it can be observed that the RCS for RR polarization is approximately the same as that for HH polarization, but it is greater than the results for LR polarization, which is in contrast to the results of sea surface. This may be because the ship target used in the simulation is

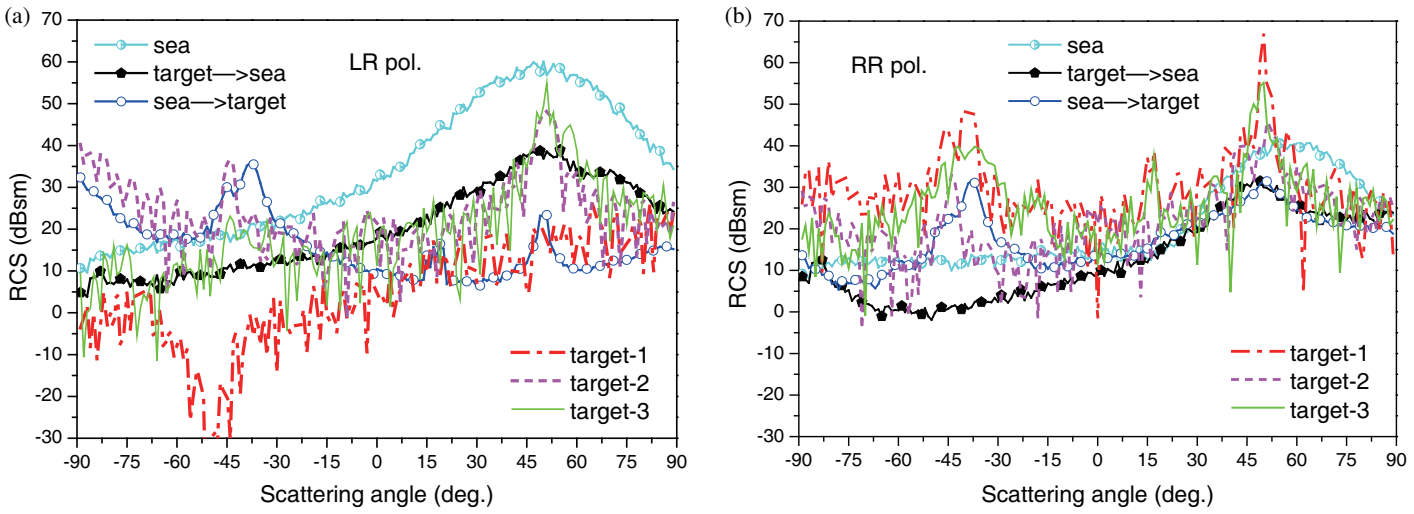

FIGURE 8. Bistatic RCS comparisons of each scattering components in the composite scene. (a) LR Polarization. (b) RR Polarization.

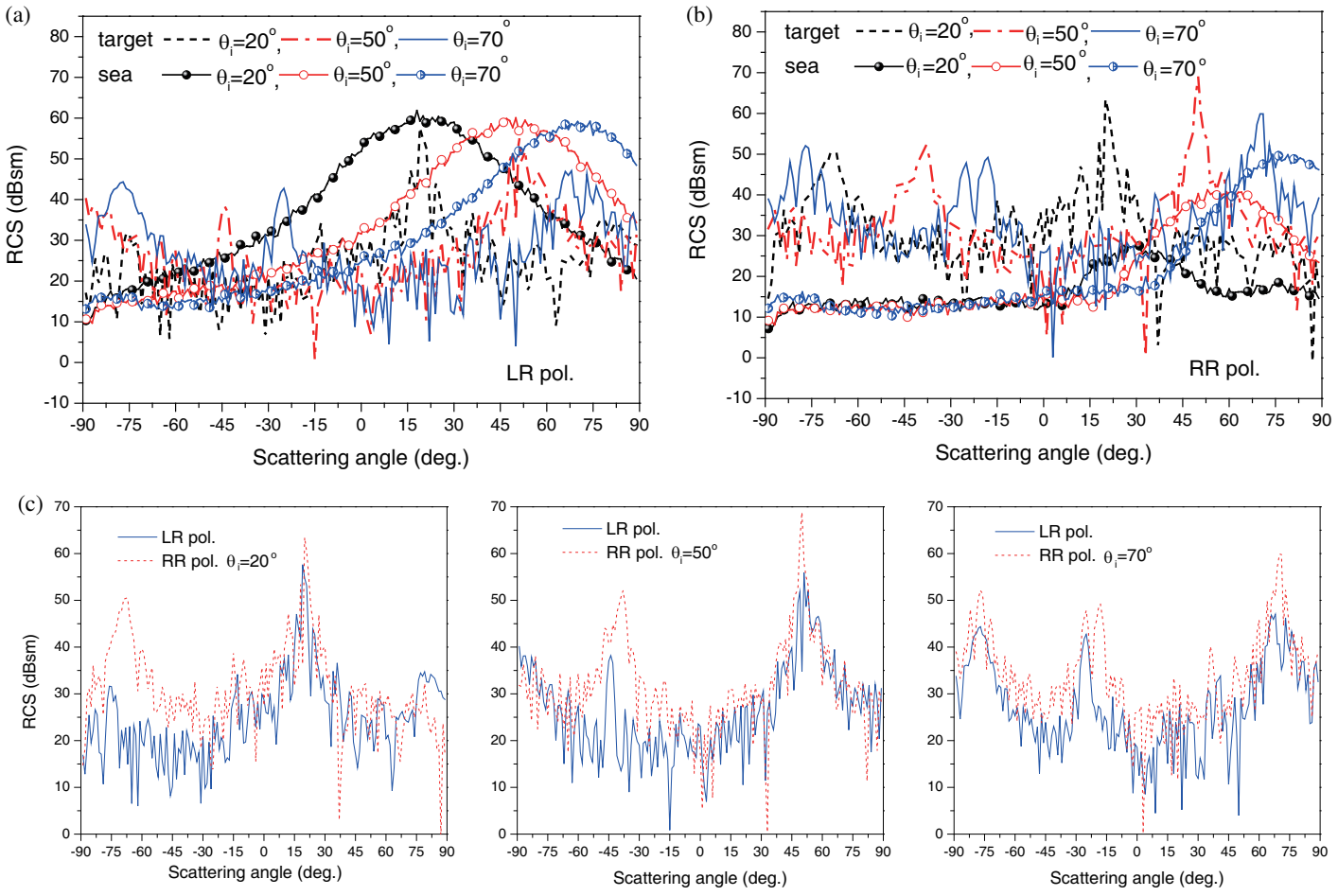

FIGURE 9. Bistatic RCS comparisons of sea surface and ship target at different incident angles. (a) RCS comparison of target and sea surface under LR polarization. (b) RCS comparison of target and sea surface under RR polarization. (c) RCS Comparison of target between LR and RR polarization.

perfectly electric conducting, and the ship target has a complex structure, including many angular structures, so this will cause the situation that the scattering direction deviation is serious. Therefore, for the detection and identification applications of ship target on the sea surface, in order to enhance the reception of the scattering echo of target and suppress the scattering echo of sea surface (i.e., sea clutter), the selection of the right-hand circular polarization channel is more advantageous.

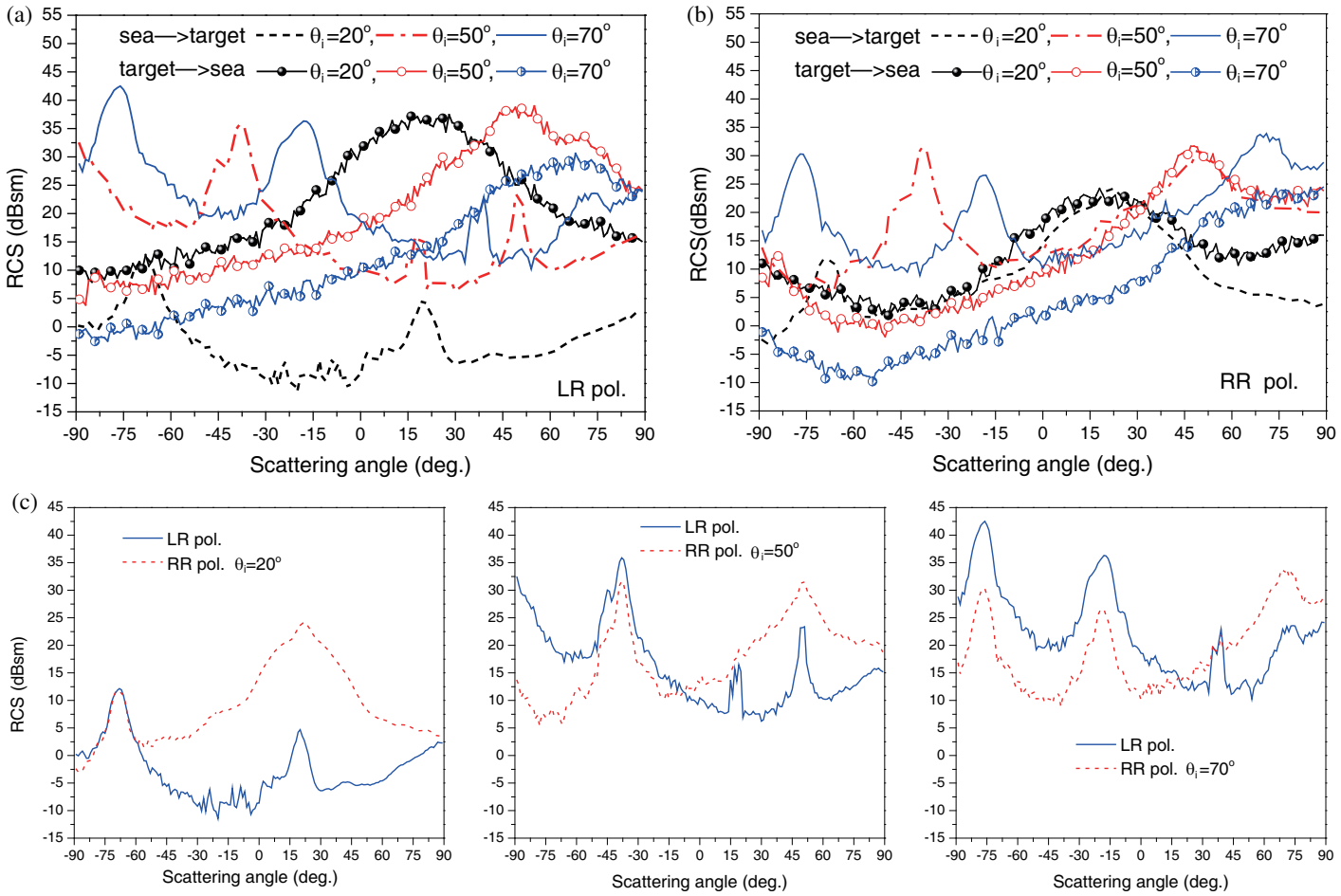

FIGURE 10. Bistatic RCS comparisons between the two coupled scattering components at different incident angles. (a) LR polarization. (b) RR polarization. (c) Comparison of the coupled scattering of target induced by the reflection waves from sea surface between LR and RR polarizations.

3.3. Composite Scattering Characteristics Analysis Between Ship Target and Sea Surface

The researches for the composite scattering characteristics between the ship target and sea surface are given in this section. Fig. 8 illustrates the variation of each scattering component with the scattering angle in the composite scene. The incident angle is $\theta_i = 50°$; the incident azimuth angle is $\phi_i = 0°$; the scattering azimuth angle is $\phi_s = 0°$; wind speed is 5 m/s; and wind direction and heading are $0°$.

From Fig. 8(a), it can be observed that the first-order scattering of target for the LR polarization has a very small magnitude, which is smaller than the magnitudes of the second and third-order scattering components. In the backscattering region, the contributions both for the second-order scattering of target and for the coupled scattering of target caused by the reflection wave from the sea surface are greater than the scattering contribution from sea clutter. Moreover, the coupled scattering of sea surface caused by the reflection wave from the target is significantly smaller than the scattering of sea surface. From Fig. 8(b), one can observe that the first-order scattering of target for the RR-polarization is greater than the second and third-order scattering components. At certain scattering angles, the results of third-order scattering of target exceed those of second-order scattering. Because the scattering level of sea surface for the RR polarization is relatively small on the whole, the first, second, and third-order scattering results from the target are greater than those from the sea surface. In the backscattering region, the coupled scattering of target induced by the reflection wave from sea surface is also greater than the scattering results from sea surface. Additionally, comparing Figs. 8(a) with (b), it can also be observed that it is better to choose the right-hand circular polarization channel to receive the scattering echo signal of the target.

Figure 9 provides the comparisons of the bistatic RCS for the sea surface and ship target at different incident angles with incident azimuth angle of $\phi_i = 0°$, scattering azimuth angle of $\phi_s = 0°$, wind speed of 5 m/s, and wind direction and heading of $0°$. From Figs. 9(a) and (b), it can be seen that in the backscattering region, as the incident angle decreases, the scattering of sea surface increases under LR polarization, while it remains essentially the same under RR polarization. In the forward direction, both for the LR polarization and RR polarization, the scattering of sea surface increases with the increase of incident angle. Comparing the scattering of sea surface with target, the scattering of target is significantly greater than that of sea surface under RR polarization. However, for the LR polarization, the echo signal of target is basically drowned out by

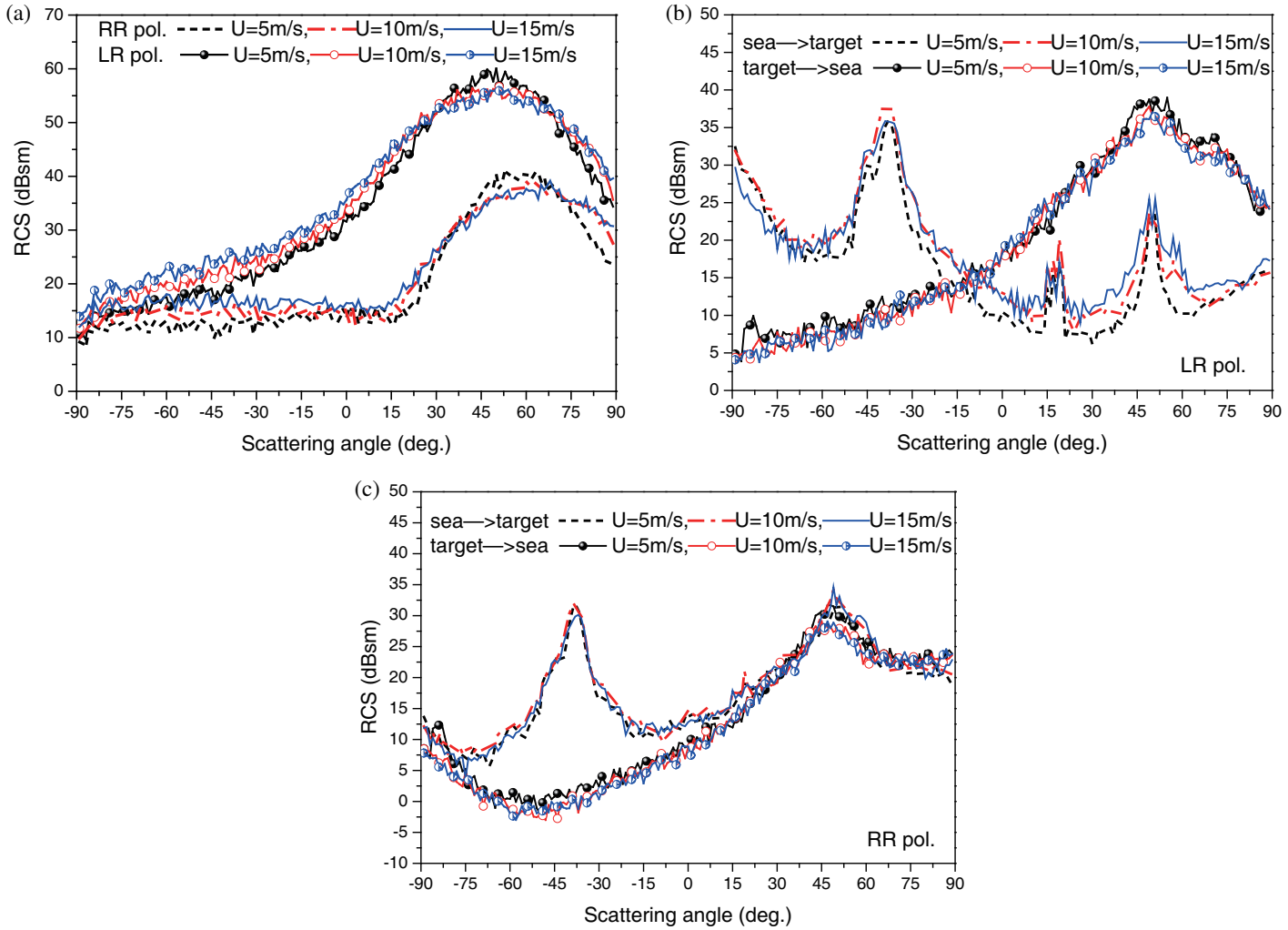

FIGURE 11. Bistatic RCS comparisons of sea surface and coupled scattering components at different wind speeds. (a) Sea surface. (b) Coupled scattering under LR polarization. (c) Coupled scattering under RR polarization.

sea clutter. From Fig. 9(c), with the incident angle increasing, the number of scattering peaks increases for both the LR polarization and RR polarization. From the location viewpoint, the scattering peak positions of target for RR polarization coincide with those for LR polarization. However, from the magnitude perspective, the scattering peak values for RR polarization are greater than those for LR polarization. In short, at the same incident angle, the scattering of target under RR polarization is larger than that under LR polarization on the whole.

Figure 10 presents the comparisons of bistatic RCS between the two coupled scattering components at different incident angles. The simulation parameters are the same as those in Fig. 9. From Figs. 10(a) and (b), it can be observed that in the backscattering region, for both LR and RR polarizations, the coupled scattering of sea surface induced by the reflection waves from target decreases with the increasing of incident angle. Comparing the two coupled components, as the incident angle increases, the coupled scattering of target induced by the reflection waves from sea surface (i.e., sea —> target) will become greater than the coupled scattering of sea surface induced by the reflection waves from target (i.e., target —> sea). Moreover, the larger the incident angle is, the more pronounced this phenomenon becomes. From Fig. 10(c), it can be observed that in the vicinity of the mirror direction, the coupled scattering of target induced by the reflection waves from sea surface under RR polarization is greater than that under LR polarization. In the backscattering region, the results for LR polarization are greater than those for RR polarization, and the larger the incident angle is, the greater the amplitude increases between the LR polarization and RR polarization.

Figure 11 gives the comparisons of bistatic RCS of sea surface and coupled scattering components at different wind speeds. The incident angle is $\theta_i = 50°$; the incident azimuth angle is $\phi_i = 0°$; the scattering azimuth angle is $\phi_s = 0°$; and both the wind direction and heading are $0°$. From Fig. 11(a), it can be observed that for both RR and LR polarizations, the scattering of sea surface increases with the increasing of wind speed, except in the mirror direction, where it decreases with the increase of wind speed. From Figs. 11(b) and (c), one can see that the coupled scattering of sea surface induced by the reflection waves from target also decreases with the increase of wind speed in the vicinity of the mirror direction, which is similar to

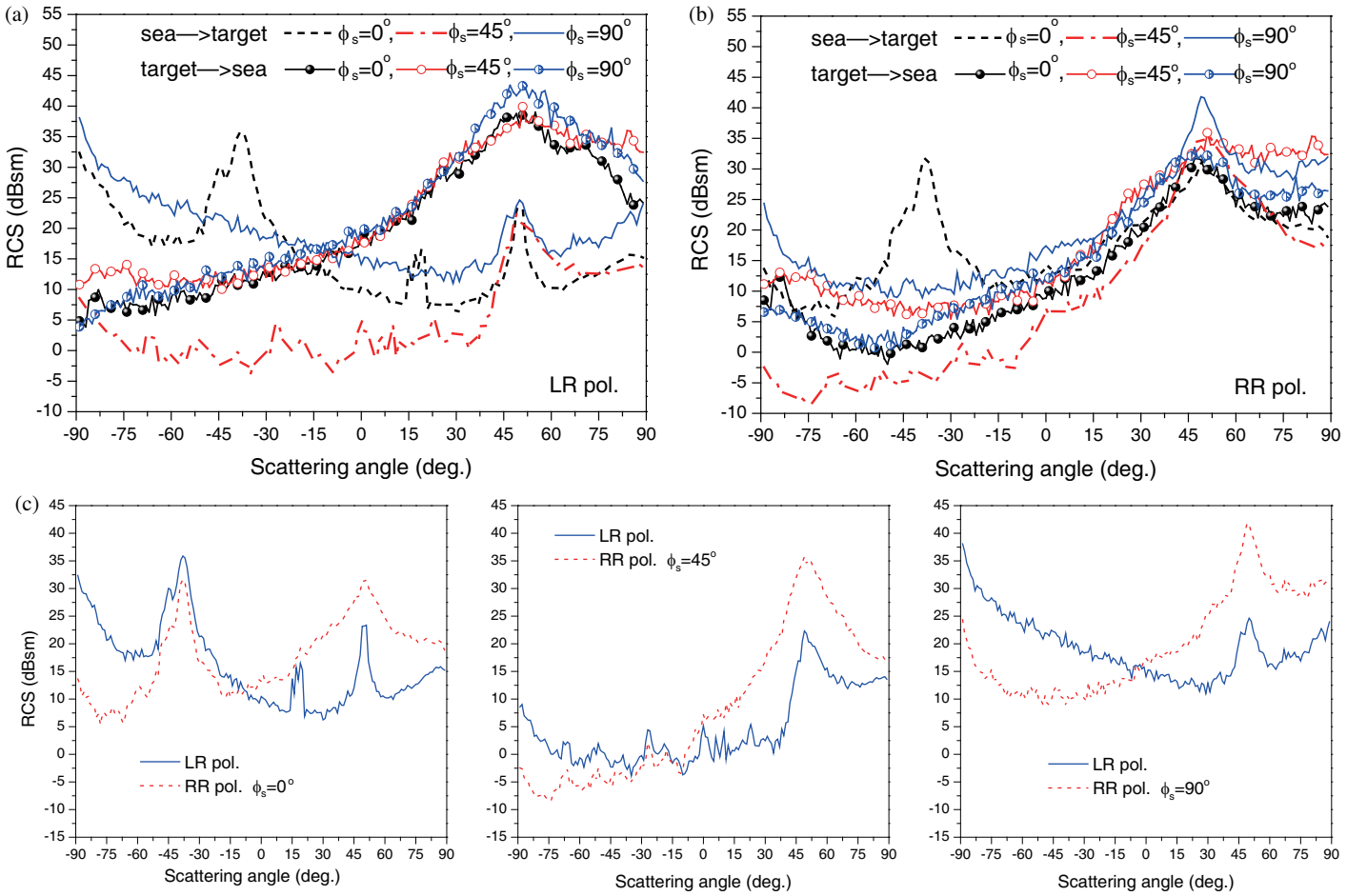

FIGURE 12. Bistatic RCS comparisons between the two coupled scattering components at different ship headings. (a) Coupled scattering under LR polarization. (b) Coupled scattering under RR polarization. (c) Comparisons of the coupled scattering of target induced by the reflection waves from sea surface between LR and RR polarizations.

the case of sea surface. For the LR polarization, the coupled scattering of target induced by the reflection waves from sea surface increases with the increase of wind speed in the vicinity of the mirror direction, while for the RR polarization, the results are less sensitive to wind speed. In summary, on the whole, the effect of wind speed on both the scattering of sea surface and the coupled scattering appears relatively modest. Comparing the coupled scattering of target induced by the reflection waves from sea surface for the two polarizations, the result under RR polarization is greater than that under LR polarization in the forward direction, while the backscattering result has opposite situation, as seen in Fig. 10(c) (i.e., the middle figure, $\theta_i = 50°$, the wind speed is 5 m/s). And this conclusion holds for different wind speeds.

Figure 12 displays the comparisons of the bistatic RCS between the two coupled scattering components at different ship headings. The incident angle is $\theta_i = 50°$; the incident azimuth angle is $\phi_i = 0°$; the scattering azimuth angle is $\phi_s = 0°$; the wind speed is 5 m/s; and the wind direction is $0°$. From Figs. 12(a) and (b), it can be observed that in the vicinity of the mirror direction, the coupled scattering of target induced by the reflection waves from sea surface increases with the increase of heading angle for the two polarizations. Except the mirror direction, the results are noticeably small when the heading is $45°$. When the heading is $0°$, there is a peak in the backscattering direction, and under LR polarization this peak value is greater than the peak value at mirror direction. With the change of heading, the coupled scattering of sea surface induced by the reflection waves from target does not exhibit a consistent pattern. For LR polarization, the results at the heading of $90°$ are slightly larger than the results at the other two headings. For RR polarization, the results at the heading of $0°$ are generally smaller than the results at the other two headings. From Fig. 12(c), it can be found that $\theta_s = 0°$ serves as a turning point, and for $\theta_s > 0°$, the coupled scattering of target induced by the reflection waves from sea surface under RR polarization is greater than that under LR polarization, while for $\theta_s < 0°$, it has just the opposite conclusion.

Figure 13 shows the comparisons of the bistatic RCS of ship target at different headings. The simulation parameters are the same as those in Fig. 12. From Figs. 13(a) and (b), it can be observed that, for both the polarizations, the results at the heading of $45°$ are significantly smaller than those for the other two heading directions. Except for some certain scattering angles, the results at the heading of $90°$ are greater than those at the heading of $0°$.

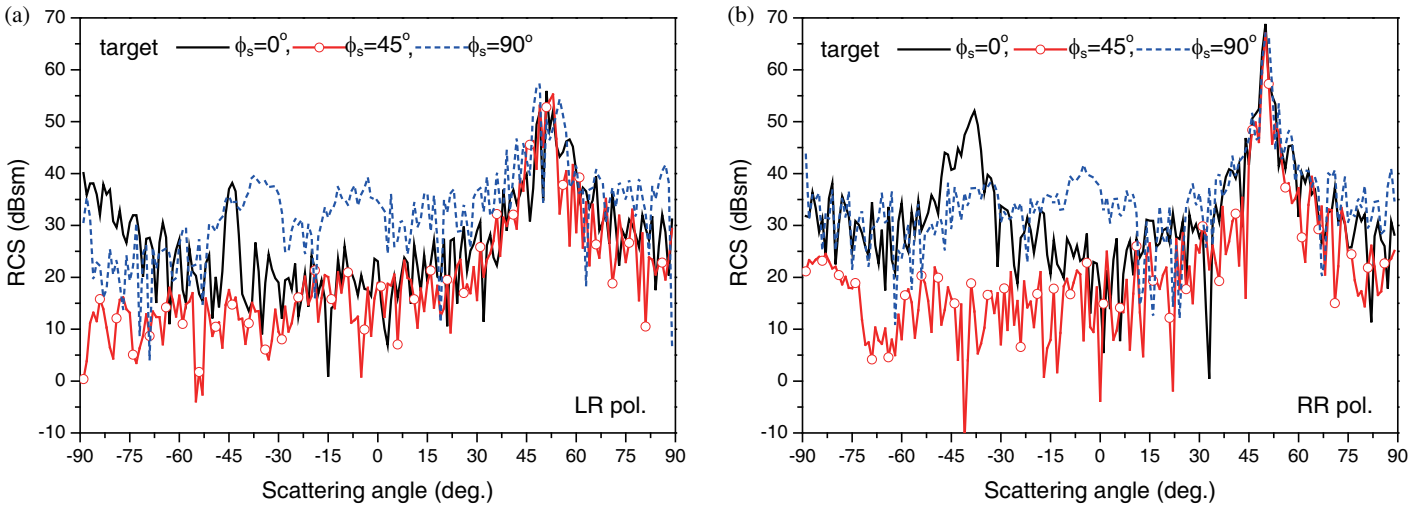

FIGURE 13. Bistatic RCS comparisons for ship target at different ship headings. (a) LR polarization. (b) RR polarization.

4. CONCLUSION

This study provides an exhaustive analysis of the composite scattering characteristics of the sea surface and ship target at GPS frequency under circular polarization. For this purpose, a comprehensive composite scattering model is established to investigate the composite scattering characteristics under various conditions, which uncovers the significant differences in the scattering behaviors of the different scattering components under different polarization states. This work reveals the complex interactions in the complex scene with sea surface and overlying ship target, which can significantly enhance our understanding for the scattering phenomena at GPS frequency and underscore the importance of polarization analysis in the study of composite scattering characteristics. Moreover, this work not only enriches the theoretical knowledge in the field, but also has potential applications in enhancing the accuracy and reliability of maritime surveillance and remote sensing technologies.

ACKNOWLEDGEMENT

This work was supported in part by the National Natural Science Foundation of China (Grant Nos. 62261054, 62361054 and 62061048), in part by the Shaanxi Key Research and Development Program (Grant No. 2024GX-YBXM-108), and in part by the Research project of Yan'an University (Grant No. 2023JBZR-009).

REFERENCES

[1] Li, J., L. Zhang, and Q. Qin, "A regularized fast multipole method of moments for rapid calculation of three-dimensional time-harmonic electromagnetic scattering from complex targets," *Engineering Analysis with Boundary Elements*, Vol. 142, 28–38, Sep. 2022.

[2] Lu, E., W. Ren, H. Dai, and X. Zhu, "Investigations on electromagnetic wave scattering simulation from rough surface: Some instructions for surface roughness measurement based on machine vison," *Precision Engineering*, Vol. 82, 156–168, Jul. 2023.

[3] Ye, L., S. Hu, G. Xu, and T. Yan, "A meshless regularized method of fundamental solution for electromagnetic scattering problems of three-dimensional perfect electric conductor targets," *Engineering Analysis with Boundary Elements*, Vol. 155, 401–406, Oct. 2023.

[4] Zhao, R., Z. X. Huang, Y. P. Chen, and J. Hu, "Solving electromagnetic scattering from complex composite objects with domain decomposition method based on hybrid surface integral equations," *Engineering Analysis with Boundary Elements*, Vol. 85, 99–104, Dec. 2017.

[5] Burkholder, R. J., M. R. Pino, and F. Obelleiro, "A Monte Carlo study of the rough-sea-surface influence on the radar scattering from two-dimensional ships," *IEEE Antennas and Propagation Magazine*, Vol. 43, No. 2, 25–33, Apr. 2001.

[6] Zhang, M., W. Luo, J.-T. Liu, L. Bai, and P. Zhou, "Method of fundamental solution for composite electromagnetic scattering from two-dimensional object located on a rough surface," *Chinese Physics Letters*, Vol. 27, No. 1, 014101, Jan. 2010.

[7] Colak, D., R. J. Burkholder, and E. H. Newman, "Multiple sweep method of moments (MSMM) analysis of electromagnetic scattering from targets on ocean-like rough surfaces," in *IEEE Antennas and Propagation Society International Symposium. Transmitting Waves of Progress to the Next Millennium. 2000 Digest. Held in conjunction with: USNC/URSI National Radio Science Meeting (C*, 2124–2127, Salt Lake City, UT, USA, Jul. 2000.

[8] Zhang, Y., J. Lu, J. Pacheco, C. D. Moss, C. O. Ao, T. M. Grzegorezyk, and J. A. Kong, "Mode-expansion method for calculating electromagnetic waves scattered by objects on rough ocean surfaces," *IEEE Transactions on Antennas and Propagation*, Vol. 53, No. 5, 1631–1639, May 2005.

[9] Kuang, L. and Y.-Q. Jin, "Bistatic scattering from a three-dimensional object over a randomly rough surface using the FDTD algorithm," *IEEE Transactions on Antennas and Propagation*, Vol. 55, No. 8, 2302–2312, Aug. 2007.

[10] Wei, Y.-W., L.-X. Guo, A.-Q. Wang, and Z.-S. Wu, "Application of multiregion model to EM scattering from a dielectric rough surface with or without a target above it," *IEEE Transactions on Antennas and Propagation*, Vol. 61, No. 11, 5607–5620, Nov. 2013.

[11] Chiu, T. and K. Sarabandi, "Electromagnetic scattering interaction between a dielectric cylinder and a slightly rough surface," *IEEE Transactions on Antennas and Propagation*, Vol. 47, No. 5,

902–913, May 1999.

[12] Lawrence, D. E. and K. Sarabandi, "Electromagnetic scattering from a dielectric cylinder buried beneath a slightly rough surface," in *IEEE Antennas and Propagation Society International Symposium. 2001 Digest. Held in conjunction with: USNC/URSI National Radio Science Meeting (Cat. No.01CH37229)*, Vol. 4, 348–351, Boston, MA, USA, 2001.

[13] Johnson, J. T., "A study of the four-path model for scattering from an object above a half space," *Microwave and Optical Technology Letters*, Vol. 30, No. 2, 130–134, Jul. 2001.

[14] Johnson, J. T., "A numerical study of scattering from an object above a rough surface," *IEEE Transactions on Antennas and Propagation*, Vol. 50, No. 10, 1361–1367, Oct. 2002.

[15] Burkholder, R. J., M. R. Pino, and D. H. Kwon, "Development of ray-optical methods for studying the RCS of 2D targets on a rough sea surface," *The Ohio State University Electroscience Laboratory Technical Report*, 735 231–1, 1999.

[16] Burkholder, R. J., P. Janpugdee, and D. Colak, "Development of computational tools for predicting the radar scattering from targets on a rough sea surface," *Final Report No. XBONR*, 2001.

[17] Di Martino, G., A. D. Simone, W. Fuscaldo, A. Iodice, D. Riccio, and G. Ruello, "Electromagnetic scattering from a canonical target over an anisotropic rough surface using geometrical optics," in *2020 XXXIIIrd General Assembly and Scientific Symposium of the International Union of Radio Science*, 1–4, Rome, Italy, 2020.

[18] Zhao, H., L.-X. Guo, and S.-H. Liu, "EM scattering of a target over sea surface based on physical optics," in *Proceedings of 2014 3rd Asia-Pacific Conference on Antennas and Propagation*, 1098–1101, Harbin, China, Jul. 2014.

[19] Zhou, C., H. Zi, T. Sun, D. Ding, and R. Chen, "A local current based iterative physical optics method for computing the RCS of target above sea surface," *Engineering Analysis with Boundary Elements*, Vol. 146, 318–326, Jan. 2023.

[20] Zhang, M., Y. Zhao, J.-X. Li, and P.-B. Wei, "Reliable approach for composite scattering calculation from ship over a sea surface based on FBAM and GO-PO models," *IEEE Transactions on Antennas and Propagation*, Vol. 65, No. 2, 775–784, Feb. 2017.

[21] Zhao, Y., X.-C. Ren, and P.-J. Yang, "Study on the composite EM scattering from sea surface with ship based on kd-tree accelerated hybrid model," *International Journal of Antennas and Propagation*, Vol. 2019, Article ID 9816829, Oct. 2019.

[22] Xu, F. and Y.-Q. Jin, "Bidirectional analytic ray tracing for fast computation of composite scattering from electric-large target over a randomly rough surface," *IEEE Transactions on Antennas and Propagation*, Vol. 57, No. 5, 1495–1505, May 2009.

[23] Bruce, N. C., "Double-scatter mueller matrices for vector electromagnetic scattering from single grooves and lines on a silicon surface," *Waves in Random and Complex Media*, Vol. 23, No. 3, 243–257, 2013.

[24] Bruce, N. C., "Multiple scatter of vector electromagnetic waves from rough metal surfaces with infinite slopes using the kirchhoff approximation," *Waves in Random and Complex Media*, Vol. 21, No. 2, 362–377, 2011.

[25] Bruce, N. C., "Double scatter vector-wave kirchhoff scattering from perfectly conducting surfaces with infinite slopes," *Journal of Optics*, Vol. 12, No. 8, 085701, 2010.

[26] He, S. Y. and G. O. Zhu, "A hybrid MM-PO method combining UV technique for scattering from two-dimensional target above a rough surface," *Microwave and Optical Technology Letters*, Vol. 49, No. 12, 2957–2960, Dec. 2007.

[27] Guan, B., J. F. Zhang, X. Y. Zhou, and T. J. Cui, "Electromagnetic scattering from objects above a rough surface using the method of moments with half-space Green's function," *IEEE Transactions on Geoscience and Remote Sensing*, Vol. 47, No. 10, 3399–3405, Oct. 2009.

[28] Yang, W., Z. Q. Zhao, C. H. Qi, W. Liu, and Z. P. Nie, "Iterative hybrid method for electromagnetic scattering from a 3-D object above a 2-D random dielectric rough surface," *Progress In Electromagnetics Research*, Vol. 117, 435–448, 2011.

[29] Bellez, S., C. Bourlier, and G. Kubické, "3-D scattering from a PEC target buried beneath a dielectric rough surface: An efficient PILE-ACA algorithm for solving a hybrid KA-EFIE formulation," *IEEE Transactions on Antennas and Propagation*, Vol. 63, No. 11, 5003–5014, Nov. 2015.

[30] Franceschetti, G., M. Migliaccio, and D. Riccio, "On ocean SAR raw signal simulation," *IEEE Transactions on Geoscience and Remote Sensing*, Vol. 36, No. 1, 84–100, Jan. 1998.

[31] Fuks, I. M. and A. G. Voronovich, "Wave diffraction by rough interfaces in an arbitrary plane-layered medium," *Waves in Random Media*, Vol. 10, No. 2, 253–272, Apr. 2000.

[32] Durden, S. L. and J. F. Vesecky, "A numerical study of the separation wavenumber in the two-scale scattering approximation (ocean surface radar backscatter)," *IEEE Transactions on Geoscience and Remote Sensing*, Vol. 28, No. 2, 271–272, 1990.

[33] Sultan-Salem, A. K. and G. L. Tyler, "Validity of the kirchhoff approximation for electromagnetic wave scattering from fractal surfaces," *IEEE Transactions on Geoscience and Remote Sensing*, Vol. 42, No. 9, 1860–1870, Sep. 2004.

[34] Voronovich, A. G. and V. U. Zavorotny, "Full-polarization modeling of monostatic and bistatic radar scattering from a rough sea surface," *IEEE Transactions on Antennas and Propagation*, Vol. 62, No. 3, 1362–1371, Mar. 2014.

[35] Fung, A. K., *Microwave Scattering and Emission Models and Their Applications*, Artech House, Boston, 1994.

[36] Gordon, W., "Far-field approximations to the Kirchoff-Helmholtz representations of scattered fields," *IEEE Transactions on Antennas and Propagation*, Vol. 23, No. 4, 590–592, 1975.

[37] Yang, P.-J., L.-X. Guo, and Q. Wang, "Circularly polarized wave scattering from two-dimensional dielectric rough sea surface," *Progress In Electromagnetics Research M*, Vol. 44, 119–126, 2015.